ARMA 21–1806

Stochastic 3D Modelling for Induced Seismicity Risk Mitigation

Eyre, T.S. and Eaton, D.W.
ASEISMIC Solutions Inc. & University of Calgary, Calgary, AB, Canada

This paper was prepared for presentation at the 55th US Rock Mechanics/Geomechanics Symposium held in Houston, Texas, USA, 20-23 June 2021. This paper was selected for presentation at the symposium by an ARMA Technical Program Committee based on a technical and critical review of the paper by a minimum of two technical reviewers. The material, as presented, does not necessarily reflect any position of ARMA, its officers, or members. Electronic reproduction, distribution, or storage of any part of this paper for commercial purposes without the written consent of ARMA is prohibited. Permission to reproduce in print is restricted to an abstract of not more than 200 words; illustrations may not be copied. The abstract must contain conspicuous acknowledgement of where and by whom the paper was presented.

ABSTRACT: Efforts to quantify induced-seismicity risk and to develop mitigation strategies are hampered by a dearth of numerical schemes that can accommodate realistic Earth models while capturing the full spectrum of applicable physics. Here we present a new approach to modelling induced seismicity, whereby the three principal mechanisms for induced-seismicity triggering are accounted for, and uncertainties in input parameters are addressed stochastically to provide a probabilistic assessment of induced-seismicity hazard. The models provide probabilities for the expected maximum magnitudes of events and the sensitivities of results to the different input parameters can be analyzed. In this manner, we can estimate the probabilities of generating an event of a certain magnitude based on the modelled injection scenario and parameter distributions. This type of modelling can be used to give a site-specific assessment of the probability of generating an induced event changes, based on different treatment designs. Case studies from western Canada are used to evaluate the applicability of this approach for unconventional oil and gas development. This methodology also has potential for mitigating injection-induced seismicity in other industries, including geothermal energy and gigatonne-scale CO_2 storage.

1. INTRODUCTION

Anthropogenic fluid injection into the subsurface is known to cause induced seismicity in some cases. Well-known examples include enhanced geothermal systems (Lee et al., 2019), wastewater disposal (Ellsworth, 2013) and hydraulic fracturing (Bao and Eaton, 2016). In the case of hydraulic fracturing, the stimulation process is designed to fracture the reservoir rocks and this induces microseismic events that are usually too small to be felt at surface ($M < 2$). Nevertheless, in rare cases, events can be large enough to exceed local regulations designed to prevent felt earthquakes. This can result in costly delays in resource extraction, moratoriums on resource development, or ultimately, infrastructure damage and human loss of life (Atkinson et al., 2020). Mitigating this issue is therefore an important goal. However, induced seismicity is a very complex problem and current mitigation strategies unfortunately have known drawbacks and therefore may not present optimal solutions to meet this objective.

Current mitigation strategies in many regions, including the Western Canadian Sedimentary Basin, use adaptive control measures known as traffic light protocols (TLPs; Kao et al., 2016, 2018; Eaton and Eyre, 2018; Shipman et al., 2018). For example, in the region of the Duvernay play close to the town of Fox Creek, Alberta, Canada, Subsurface Order No. 2 sets the yellow-light threshold (requiring a change in operations) at local magnitude 2.0, with a red-light threshold (requiring an immediate halt in operations) of local magnitude 4.0. These TLP threshold magnitude levels are higher than some other jurisdictions, but are deemed to adequately characterize the potential seismic risk in this region given the low population density (Kao et al., 2018). Similar thresholds were also adopted in NE British Columbia (BC), Canada, including the Kiskatinaw Seismic Monitoring and Mitigation Area (KSMMA). Although these protocols provide the best mitigation measures currently available, they remain imperfect, resulting in a number of due to the reactive nature of such schemes. For instance, from the introduction of the protocols in 2014 up until early 2018, three red-light events occurred each in BC and Alberta, respectively. All of the red-light events in Alberta were preceded by a yellow event, but only one red-light event in BC was preceded by such an event (Kao et al., 2018). Additionally, once an earthquake sequence is induced, events often continue after hydraulic fracturing activity has ceased. Inherent uncertainties in magnitude calculations also influence the reliability of such schemes. Kao et al., 2018 suggested several potential improvements to traffic light protocols, such as incorporating ground motion information, standardizing magnitude calculations, and adapting the traffic light

protocol to local hazard conditions. Even with these additions, some of the aforementioned problems with traffic light protocols would still exist.

Alternative mitigation approaches have focused on the statistical characteristics of seismicity to forecast maximum expected event magnitudes. Eaton and Igonin, 2018 gave an overview of the three common methods used for estimating maximum magnitudes for induced seismicity and tested them using data from western Canada. However, these approaches rely on large catalogues of seismicity to produce statistically significant results and therefore require either significant previous seismic activity in a region or high resolution, real-time monitoring networks. They also state that observations of induced seismicity from hydraulic fracturing in western Canada do not conform exactly with any of these models, highlighting the difficulty of using these models for maximum magnitude forecasting.

Another approach is to assess whether faults in a region are close to failure (e.g. the Fault Slip Potential (FSP) software package; Walsh and Zoback, 2016; Walsh et al., 2017). The most common method for calculating the likelihood of failure of a fault is by analyzing the proximity of a fault to failure based on the Mohr-Coulomb failure criteria (Figure 1) (Walsh and Zoback, 2016; Walsh et al., 2017). Faults that are most likely to generate an earthquake are those that are critically stressed in the regional stress field (Eaton, 2018). These critically-stressed faults are characterized by a state of incipient failure, such that a very small (relative to background stress) change in Coulomb Failure Stress (ΔCFS) is sufficient to bring a fault to a frictionally unstable state (Figure 1). Moreover, these critically-stressed faults are also more likely to generate a larger earthquake: a recent analysis that considers runaway rupture processes (Atkinson et al., 2020) suggests that rupture extending outside of a region perturbed by local stress changes only occurs if a fault is close to a critically-stressed state prior to any operations that perturb the fault stability conditions. This proximity to failure is dependent on a number of factors, including the orientation and magnitude of the stress field, the pore pressure, the orientation of the fault and properties of the fault, e.g. cohesion and coefficient of friction. These parameters are often poorly resolved, introducing large uncertainties into the analysis.

In order to overcome this inherent uncertainty, the FSP software (Walsh and Zoback, 2016; Walsh et al., 2017) takes a stochastic approach, wherein a large number of realizations are computed within a numerical simulation framework. This allows for a probabilistic assessment of the likelihood of generating an earthquake on predefined faults based on the assumed realistic ranges of input parameters. However, the approach of the FSP software was designed primarily for wastewater disposal wells and can therefore prove difficult to apply to hydraulic fracturing-induced seismicity. For example, it relies solely on the effects of pore pressure diffusion (i.e. neglects other potentially important mechanisms such as poroelastic stress effects) and models injections as point sources. This approach also provides no information on likely maximum event magnitudes, and the authors have noted that earthquakes often occur on previously unidentified faults, while in many cases no events occur on faults that show high fault slip potential.

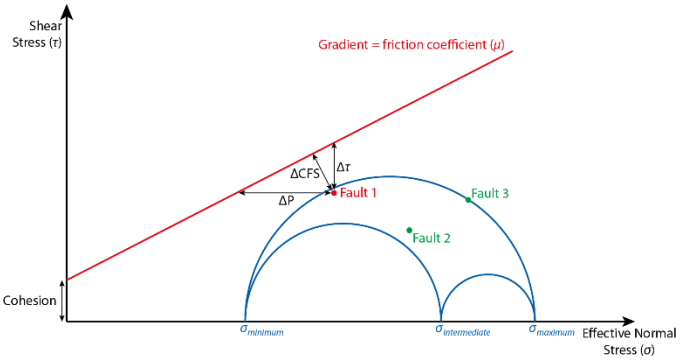

Figure 1. Schematic Mohr diagram showing state of stress for three faults. The Coulomb failure criterion is shown in red and is a function of the friction coefficient and the cohesion. Failure can occur on Fault 1 if the pore pressure (and/or effective normal stress) changes by ΔP, or if the shear stress changes by $\Delta\tau$. These effects can be combined into the Coulomb failure stress change required to slip (ΔCFS). If $\Delta CFS \leq 0$, the fault is critically stressed. In the diagram, Fault 1 is closer to slip than the other faults. Faults 2 and 3 have an equal ΔCFS and ΔP.

The method described here aims to provide an alternative, improved approach for induced seismicity mitigation. The objective is to create a software toolbox that can aid in producing site-specific quantitative mitigation and response plans by combining reservoir-simulation methods with advanced geomechanical and seismological computational tools. This software is currently in the development phase, with a number of modules that are at or nearing completion.

We give a high-level overview of progress to-date and show synthetic examples based on a real case study. Our work so far has predominantly focused on hydraulic fracturing-induced seismicity, but there is clear potential to extend these methods to other injection-induced seismicity applications (e.g. CO_2 sequestration, engineered geothermal systems, etc.).

2. TRIGGERING MECHANISMS

Modelling of induced seismicity is complicated by the fact that several models have been proposed to explain the mechanisms of fault activation by hydraulic fracturing (Eyre et al., 2019b). The most common is an increase in pore pressure within the fault zone, which leads to a reduction in effective normal stress acting on the fault (Bao and Eaton, 2016). Alternatively, poroelastic

coupling between pore pressure and the rock matrix is capable of altering fault-loading conditions without any hydraulic connection (Segall and Lu, 2015; Kettlety et al., 2020). A new model was recently suggested by Eyre et al., 2019b for hydraulic fracturing-induced seismicity, whereby aseismic fault slip may play a major role. According to this model, distal, unstable regions of a fault are progressively loaded by aseismic slip on proximal, stable regions of the fault that are stimulated by pore pressure and/or stress changes due to fluid injection. This has significant implications for the mitigation of induced seismicity, as it suggests that there is a measurable slow slip/deformation signal ~ hours prior to the nucleation of an induced earthquake, which may aid monitoring and mitigation efforts. Additionally, if we better understand the driving processes, we can improve models that can be used to simulate injection scenarios.

Most of the current modelling strategies focus on either pore pressure or poroelastic stress changes, depending on which is deemed to have a more important effect in each individual case. Additionally, they generally neglect the possibility that faults can slip either seismically or aseismically, depending on a number of different factors. It is important to incorporate all of these elements into modelling efforts, and thus our approach combines all of these effects.

3. MODELLING APPROACH AND EXAMPLES

We take a novel approach to modelling in order to aid mitigation efforts. This leverages some elements of the approach used in the FSP package, but extends the approach in an attempt to overcome some of the limitations of this method that were previously described. For example, the modelling is fully 3D and allows for the estimation of maximum expected event magnitudes. It also takes into account the three proposed mechanisms for hydraulic fracturing-induced seismicity described in the previous section.

Like FSP, we use a stochastic approach due to the inherent uncertainties in many of the parameters. This also allows for presentation of results in a probabilistic framework, which is important for hazard assessment. Simulations can be executed for a large number of iterations of input parameters that are assigned stochastically from distributions, which are assigned based on the available knowledge of the area.

4. FAULT MODELS

The software allows for the loading of time or depth-converted fault picks from 3D seismic data. Time picks are converted to depth using loaded time-to-depth conversion curves. The software converts these 3D depth-converted fault picks into 3D gridded fault models by interpolating between these picks, with a grid spacing assigned by the user. An example for a single fault is shown in Figure 2, but much more complex models that incorporate multiple faults can be analyzed.

5. STRESS MODELS

Construction of a realistic depth-dependent stress model is important in this approach. To analyze the proximity of faults in a region to slip, the effective stress acting on the fault needs to be evaluated (Figure 1). The effective stress is defined as:

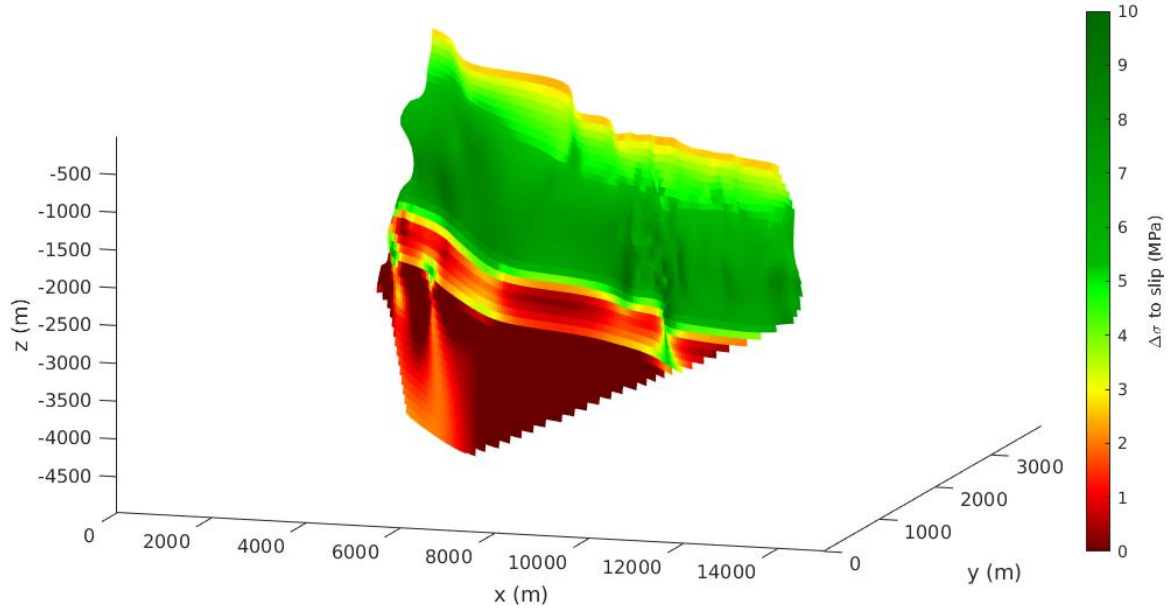

Figure 2. Example of a 3D model of fault slip potential (plotted as change in normal stress required for slip) for a fault interpreted from 3D seismic data. Note that the regional stress model contains two distinct overpressured layers, which cause the deeper parts of the fault to be close to failure.

$$\sigma_{eff} = \sigma_n - \beta P, \quad (1)$$

where σ_n is the normal stress, β is the Biot parameter and P is the pore pressure. In many cases the Biot coefficient is approximated to be 1; however, this is a simplification (Li et al., 2019) that can have an important influence on the estimation of effective stress. Figure 3 shows examples of synthetic stress profiles, a pore pressure profile including an overpressured zone at depth and the corresponding effective stress profiles. The zone of pore overpressure has a strong influence on the profiles by dramatically reducing the effective stresses, which will bring any faults closer to failure at these levels. Figure 2 shows a fault with two layers of increased pore overpressure at depth, demonstrating how this overpressure increases the potential for slip. We are also integrating stress as a function of rock strength when creating stress profiles, as this can vary significantly in sedimentary stratigraphy (Roche and van der Baan, 2015).

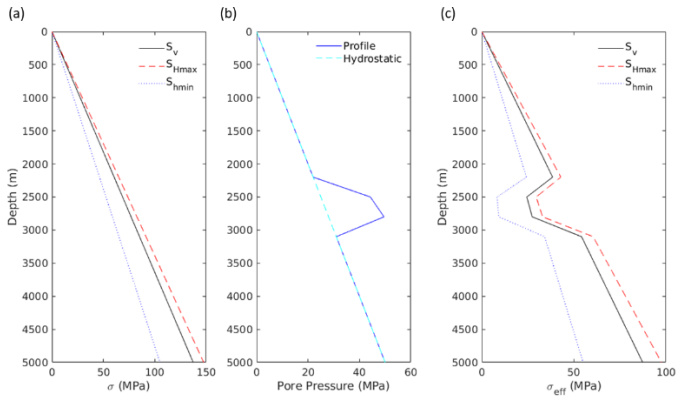

Figure 3. Synthetic example of stress profiles required in the modelling. (a) Simple stress profiles constructed from estimated stress gradients. (b) Example pore pressure profile similar to that of Eyre et al., 2019b for the Duvernay play near Fox Creek, AB. The reservoir is modelled as an overpressured zone. (c) Effective stress profile constructed from (a) and (b). The overpressure greatly reduces the effective stress, bringing any faults passing through this zone closer to failure.

Orientations for the principal horizontal stress S_{Hmax} can be estimated for a region based on a variety of techniques such as wellbore deformation orientations (i.e. tensile drilling-induced fractures and borehole breakouts) and stress inversions from earthquake focal mechanisms (Zhang et al., 2019). A globally compiled database for these orientations is available from the World Stress Map (Heidbach et al., 2016), although the reliability of such data can vary depending on the data density in the region being studied.

6. FAULT SLIP POTENTIAL ANALYSIS

In order to analyze the fault slip potential in a probabilistic sense, the simulations are performed a large number of times using a stochastic approach. During each iteration, every unknown parameter in the model (e.g. cohesion, coefficient of friction (μ), shear modulus (G), pore pressure, stress and S_{Hmax} orientation) is varied within a priori range to produce a large number of outcomes which can be analyzed probabilistically. A practical requirement is computational efficiency, in order for the software to produce a result within a reasonable timeframe and/or at reasonable computational expense. Our current approach to simulating injection scenarios and the resulting stress and pore pressure changes is therefore deliberately simple, but nevertheless captures key dynamic behavior of more complex models given the stochastic nature of our approach.

Realistic distributions of input parameters are used as inputs into the model (Figure 4). Calculations are iterated for a large number (e.g. 10,000) of times to provide a probabilistic assessment of fault stability. For each iteration, we calculate the maximum expected magnitude of an event caused by the modelled effective stress acting on any of the modelled faults.

In this manner, we can estimate the probability distribution of generating an event of a certain magnitude based on the modelled injection scenario and parameter distributions. Figure 5 shows an example of the results of a model that was ran for 10,000 iterations. It is apparent that the probability of occurrence of earthquakes in this scenario is low and the vast majority of the 10,000 model runs produced no earthquakes. Based on the obtained results, we can estimate that the probability of a magnitude 2.0 event is 0.0072 and a magnitude 3.0 event is 0.0002.

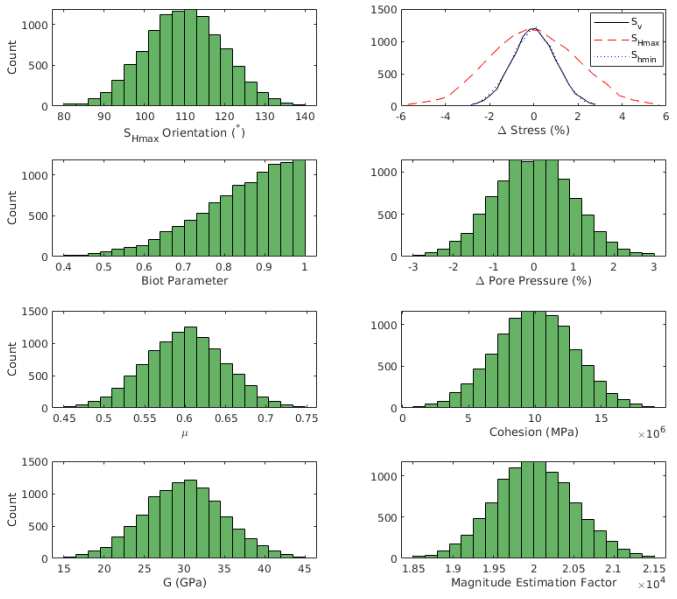

Figure 4. Example of input parameter distributions for the stochastic modelling. Parameters are explained in more detail in the text.

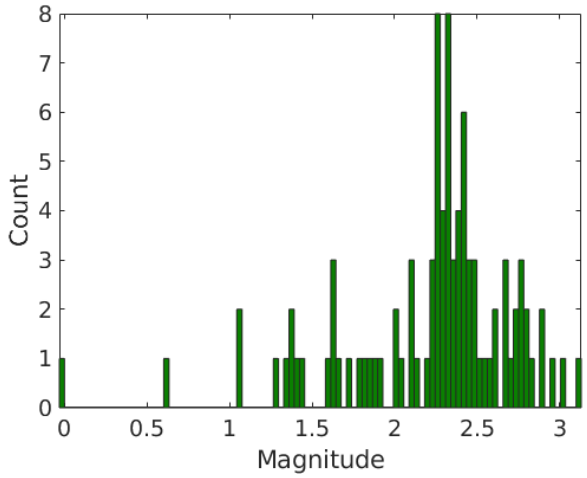

Figure 5. Example of a histogram of the maximum earthquake magnitude results produced by the stochastic modelling. Note that 10,000 iterations were carried out, so the vast majority of simulations produce no significant induced seismicity.

The sensitivities of the results to the input parameters can also be analysed using tornado plots (Figure 6). This diagram shows the variability in the assigned inputs and the sensitivities of the calculated maximum magnitudes. In the example shown, the strongest influence is cohesion, which has a large impact on the position of the failure envelope (Figure 1). However, this parameter is poorly constrained and therefore has a wide input distribution, which influences the sensitivity shown here. The parameter that appears to show the most sensitivity is S_{hmin}, which shows a wide range of magnitudes despite a narrow input distribution. It is interesting that μ, which was also expected to have a strong influence on the proximity of the fault to failure (Figure 1), shows one of the smallest sensitivities in the case shown here, despite significant input variability.

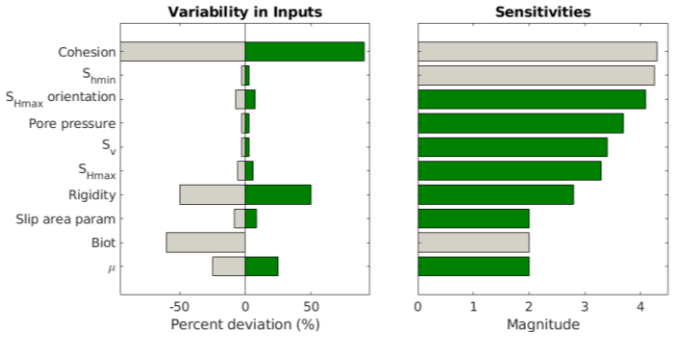

Figure 6. Example of a tornado plot to show the sensitivity of the maximum magnitude results to all of the input parameters (Figure 4) varied in the stochastic approach. Grey bars show a decrease in the parameter value while green bars show an increase. A decrease in cohesion shows the strongest influence on the maximum magnitude produced, but also had the highest included uncertainty. Variations in S_{hmin} show the strongest sensitivity.

7. OPERATIONS SIMULATIONS

Models can be ran both with and without hydraulic fracturing injection scenarios. This allows us to investigate how much difference operations are likely to make to the expected seismicity behavior within the region of interest. Hydraulic fracturing operations can be simulated by inputting the locations, timings and injection parameters of individual stages. The software has inbuilt capabilities for hydraulic fracture modelling, but can also handle outputs of more detailed hydraulic fracture modelling packages to be input into the model. Again, parameters are inputted as distributions to address the inherent uncertainties.

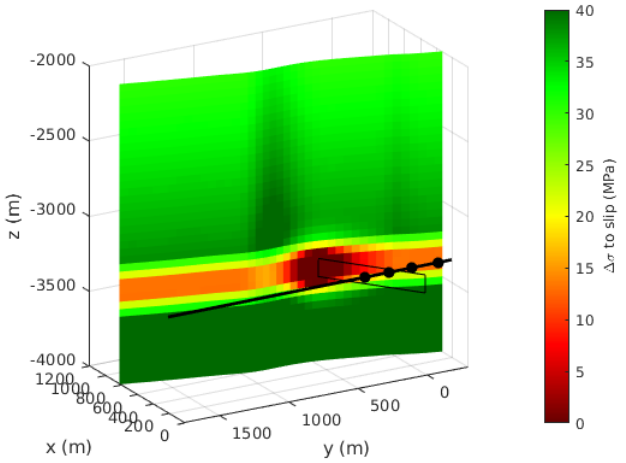

Figure 7. Example of modelling using the pressure diffusion model for a near-vertical fault. Fluid pressure leaks off from the hydraulic fracture (black rectangle) and the effect on the stability margin for the fault is shown by the color scale. The black line shows well trajectory and black circles show stages.

Figure 7 illustrates an example of the evolution of the fault stability margin on a modelled fault for one hydraulic fracture stage due to pore pressure diffusion. The increased pore pressure brings the fault closer to failure in the region close to the hydraulic fracture, the area of which is affected by the modelled diffusivity. Figure 8a shows the expected poroelastic stress changes due to a propagating hydraulic fracture, and how these stress changes can lead to variable activation of pre-existing fracture and/or fault planes. Finally, Figure 8b demonstrates how these stress changes can combine for a number of hydraulic fractures to produce a positive change in Coulomb stress in some regions on the order of megapascals. This is more than sufficient to result in fault activation, as a number of studies have suggested that stress changes caused by fluid injection of the order of 0.1 MPa are sufficiently large enough to trigger significant induced seismicity in areas where faults are critically stressed (Keranen et al., 2014; Bao and Eaton, 2016). Other studies have suggested that even stress changes of the order of 0.01 MPa are capable of triggering an earthquake (King et al., 1994; Deng et al., 2016; Ogwari

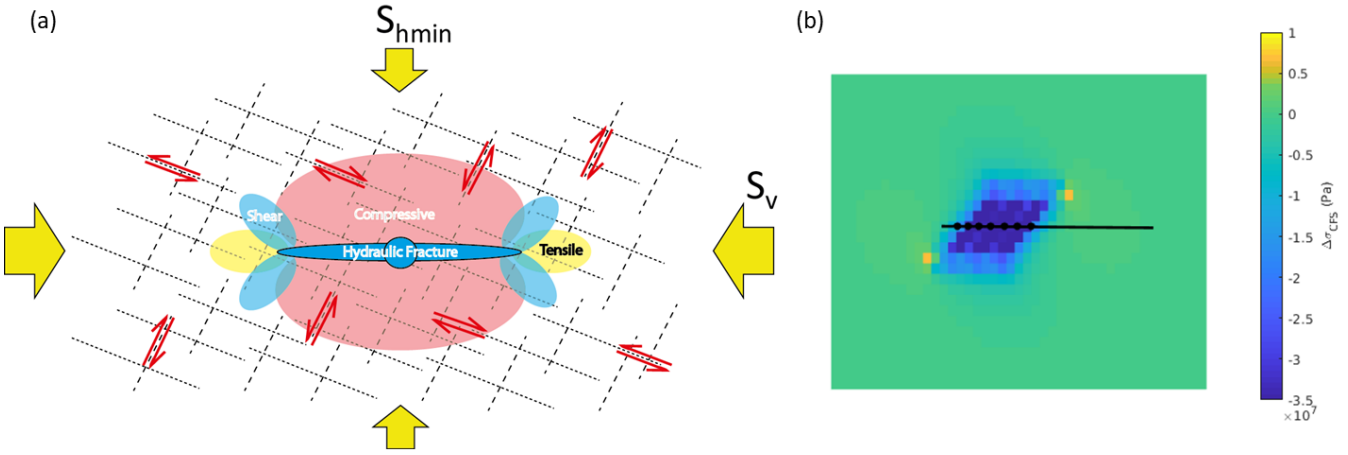

Figure 8. Example of modelling using the poroelastic stress model. (a) Expected local stress variations caused by a propagating hydraulic fracture, modified from Eyre et al. (2018). (b) Map view of the change in Coulomb stress caused by a number of hydraulic fractures for faults of a certain orientation, where positive = fault closer to failure and negative = fault further from failure. The black line shows well trajectory and black circles show stages.

and Horton, 2016). It is therefore apparent that both of these mechanisms are capable of inducing fault slip.

For further comparison, Figure 9 shows the change in Coulomb failure stress separately for pore pressure changes (for a diffusivity of 0.1 m^2/s) and poroelastic stress changes for the same modelled hydraulic fracturing treatment and fault model, based on a real treatment and associated microseismic dataset (Eyre et al., 2019a). For the input parameters analyzed here, both mechanisms produce Coulomb stress changes of a similar magnitude, emphasizing the importance of taking both mechanisms into account. Additionally, it is interesting to note that both mechanisms produce similar patterns in the Coulomb stress changes, and the highest values are quite confined in depth to regions immediately surrounding the hydraulic fractures. The combined effects of these pore pressure and stress changes on the fault slip potential are shown in Figure 10. However, Eyre et al., 2019a and Eyre et al., 2019b found that most of the microseismicity recorded during the treatment on which this model is based occurred several hundred meters above the injection well. This modelling work thus supports the aseismic slip model of Eyre et al., 2019b, as they suggested that stress and pore pressure changes due to the hydraulic fracturing would more likely lead to slip at the reservoir level than where the seismicity occurs; however, stress loading from this slip at the reservoir level (which would likely be aseismic) will load the fault in unstable regions, leading to seismicity nucleating in these zones. A key takeaway from the slip modelling work of Eyre et al., 2019b is that the majority of slip occurs in the thick carbonate formations and not where the largest pore pressure changes occur, nor where the fault is closest to failure according to the stress profile (i.e. in the reservoir formation). This demonstrates the importance of accounting for these factors in the modelling. We are currently in the process of integrating realistic slip modelling (both seismic and aseismic) into the software so that these scenarios can be more accurately modelled.

8. DISCUSSION

Our new modelling approach shows promise for modelling hydraulic-fracturing scenarios and providing results that could help to improve injection strategies to reduce the risk of induced seismicity. This modelling can be used to simulate injection programs prior to drilling to provide an assessment of the various scenarios that may result in an increased risk of induced seismicity, which will aid in the design of hydraulic fracturing treatments. Additionally, it would be advantageous in designing mitigation plans as it can assess the utility of various risk mitigation approaches (e.g. reduce pumping pressure, skip a stage, etc.). It can also be used as part of an assessment of the likelihood of induced seismicity in a new region, in tandem with an analysis of historical and background seismicity.

There are a number of advantages to this approach in comparison to existing modelling strategies. It accounts for the three possible mechanisms described by assessing stress changes due to both pore pressure changes, poroelastic effects and slip-induced stress changes, while also acknowledging that not all slip induced by these changes is likely to result in seismicity. Simulations can be ran a large number of times for input parameters that are assigned stochastically from distributions that can be based on the available knowledge of the area. The approach also provides estimates for the maximum magnitudes of any seismic events that may occur.

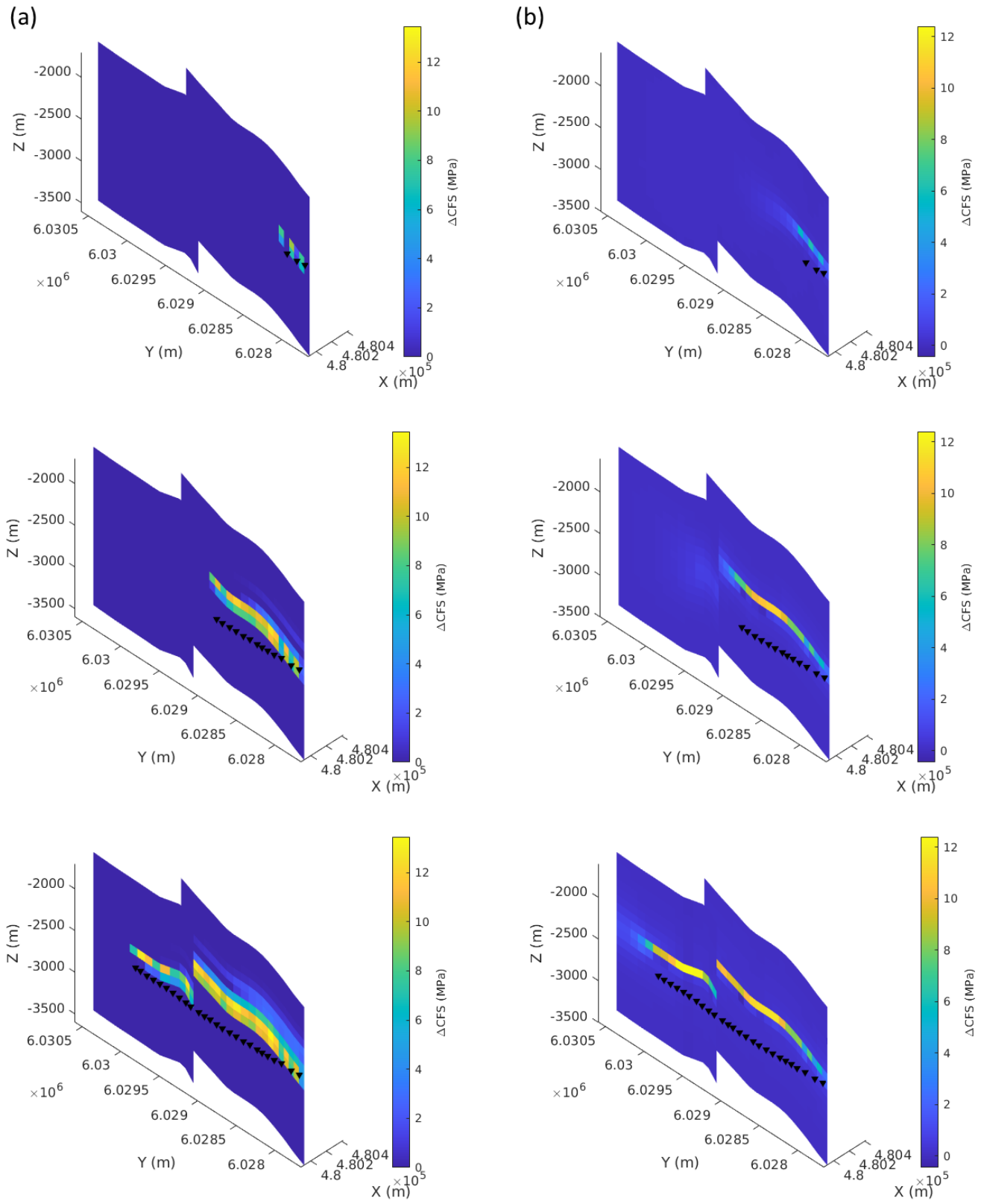

Figure 9. Example of modelling change in Coulomb failure stress due to (a) pore pressure change, and (b) poroelastic stresses caused by opening hydraulic fractures, where positive = fault closer to failure and negative = fault further from failure. Black triangles show stages; the results are shown for stages 3, 13 and 26. The fault model is based on microseismic event locations reported by Eyre et al., 2019a.

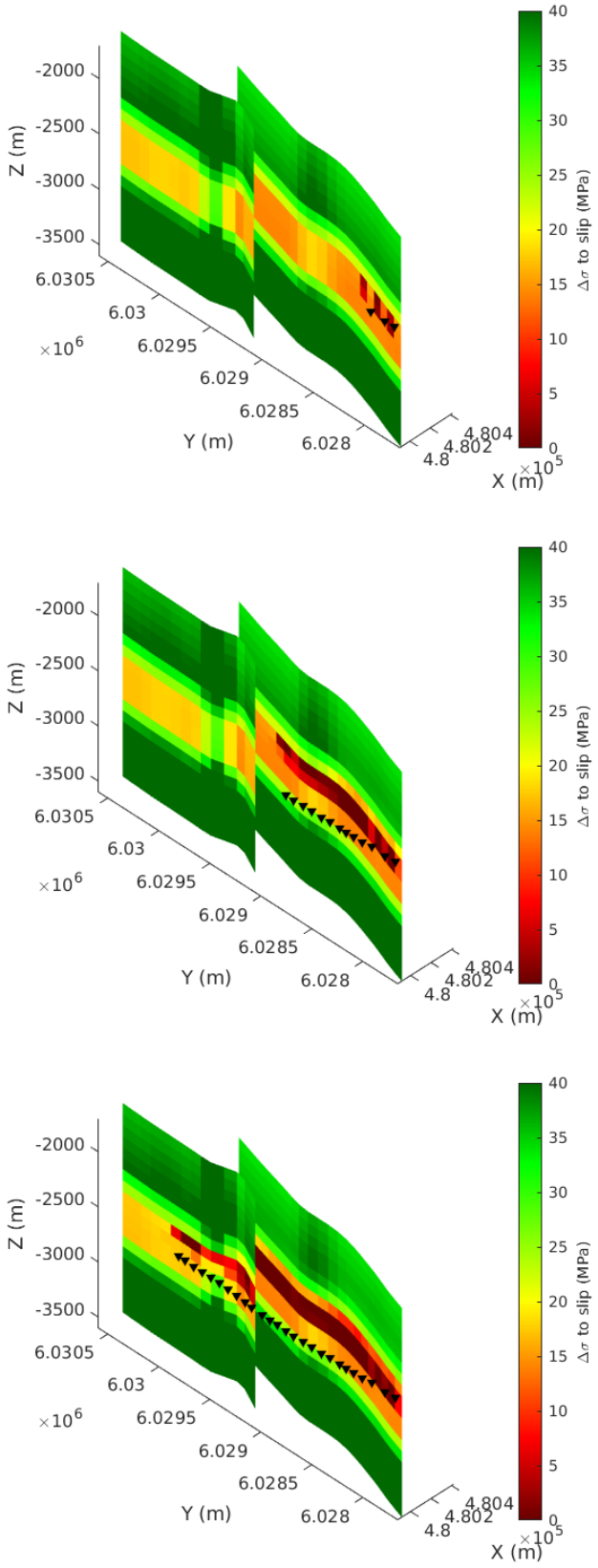

Figure 10. Example of the evolution of the fault stability margin due to the pore pressure and stress changes caused by a modelled hydraulic fracturing treatment for a fault model based on the microseismic event locations reported by Eyre et al., 2019a. Black triangles show stages; the results are shown for stages 3, 13 and 26.

9. FUTURE WORK

A number of aspects of the software are still in development, including the fault slip module that incorporates rate and state friction to allow for both aseismic and seismic slip behavior. Thorough testing utilizing various datasets is also required to both validate and optimize our approach. However, it can currently provide a much more detailed assessment of fault slip potential than other available packages. We are also working on a user-friendly graphical user interface (GUI) that will be available to run the software package. In the future, we aim to build modules that will quantify the expected ground motion and seismic hazard. This is important in induced seismicity risk mitigation as small shallow earthquakes can result in stronger ground motions than deeper, larger earthquakes, and can hence have more associated risk. We also plan to extend our methods to other induced seismicity applications, such as CO_2 sequestration and geothermal energy extraction.

10. CONCLUSION

This paper describes a new software toolbox for the hazard assessment of hydraulic fracturing-induced seismicity. The software uses a stochastic approach to provide an estimated probability distribution for the maximum expected magnitude of an induced earthquake, based on 3D analysis of fault slip potential. This can give a site-specific assessment of how the probability of generating an induced event varies based on different treatment designs. Three proposed mechanisms for induced-seismicity triggering are considered, namely pore-pressure increase, poroelastic coupling and fault loading by aseismic slip. Our approach is more comprehensive than other existing tools for hydraulic fracturing-induced seismicity.

11. ACKNOWLEDGMENTS

This research was supported in part by funding from the Canada First Research Excellence Fund. The authors would also like to thank the sponsors of the Microseismic Industry Consortium for their ongoing support.

REFERENCES

Atkinson, G. M., D. W. Eaton, and N. Igonin, 2020, Developments in understanding seismicity triggered by hydraulic fracturing: Nature Reviews Earth & Environment, **1**, 264–277.

Bao, X., and D. W. Eaton, 2016, Fault activation by hydraulic fracturing in western Canada: Science, **354**, 1406–1409.

Deng, K., Y. Liu, and R. M. Harrington, 2016, Poroelastic stress triggering of the December 2013 Crooked Lake, Alberta, induced seismicity sequence: Geophysical Research Letters, **43**, 8482–8491.

Eaton, D. W., 2018, Passive Seismic Monitoring of Induced Seismicity: Fundamental Principles and Application to Energy Technologies: Cambridge University Press, Cambridge, U.K.

Eaton, D. W., and T. S. Eyre, 2018, Induced seismicity in western Canada: causes and consequences: Geohazards 7.

Eaton, D. W., and N. Igonin, 2018, What controls the maximum magnitude of injection-induced earthquakes? The Leading Edge, **37**, 135–140.

Ellsworth, W. L., 2013, Injection-Induced Earthquakes: Science, **341**, 1–8.

Eyre, T. S., and M. Van Der Baan, 2018, Microseismic insights into the fracturing behavior of a mature reservoir in the Pembina field, Alberta: Geophysics, **83**, B289–B303.

Eyre, T. S., D. W. Eaton, M. Zecevic, D. D'Amico, and D. Kolos, 2019a, Microseismicity reveals fault activation before Mw 4.1 hydraulic-fracturing induced earthquake: Geophysical Journal International, **218**, 534–546.

Eyre, T. S., D. W. Eaton, D. I. Garagash, M. Zecevic, M. Venieri, R. Weir, and D. C. Lawton, 2019b, The Role of Aseismic Slip in Hydraulic Fracturing-Induced Seismicity:

Galis, M., J. P. Ampuero, P. M. Mai, and F. Cappa, 2017, Induced seismicity provides insight into why earthquake ruptures stop: Science Advances, **3**.

Heidbach, O., M. Rajabi, K. Reiter, and M. Ziegler, 2016, World Stress Map 2016: GFZ Data Services, doi:10.5880/WSM.2016.002.

Kao, H., R. Visser, B. Smith, and S. Venables, 2018, Performance assessment of the induced seismicity traffic light protocol for northeastern British Columbia and western Alberta: The Leading Edge, **37**, 117–126.

Kao, H., D. W. Eaton, G. M. Atkinson, S. Maxwell, and A. Babaie Mahani, 2016, Technical meeting on the traffic light protocols (TLP) for induced seismicity: summary and recommendations: , 21.

Keranen, K. M., M. Weingarten, G. A. Abers, B. A. Bekins, and S. Ge, 2014, Sharp increase in central Oklahoma seismicity since 2008 induced by massive wastewater injection: Science, **345**, 448–451.

Kettlety, T., J. P. Verdon, M. J. Werner, and J. M. Kendall, 2020, Stress Transfer From Opening Hydraulic Fractures Controls the Distribution of Induced Seismicity: Journal of Geophysical Research: Solid Earth, **125**, e2019JB018794.

King, G. C. P., R. S. Stein, and J. Lin, 1994, Static stress changes and the triggering of earthquakes: Bulletin of the Seismological Society of America, **84**, 935–953.

Lee, B. K., W. L. Ellsworth, D. Giardini, J. Townend, S. Ge, T. Shimamoto, and D. Sheen, 2019, Managing injection-induced seismic risks: Science, **364**, 730–732.

Li, Q., R. Aguilera, and H. C. Ley, 2019, A Correlation for Estimating Biot Coefficient: SPE Western Regional Meeting, SPE-195359-MS.

Ogwari, P. O., and S. P. Horton, 2016, Numerical model of pore-pressure diffusion associated with the initiation of the 2010–2011 Guy–Greenbrier, Arkansas earthquakes: Geofluids, **16**, 954–970.

Roche, V., and M. van der Baan, 2015, The role of lithological layering and pore pressure on fluid-induced microseismicity: Journal of Geophysical Research: Solid Earth, **120**, 923–943.

Segall, P., and S. Lu, 2015, Injection-induced seismicity : Poroelastic and earthquake nucleation effects: Journal of Geophysical Research : Solid Earth, **120**, 5082–5103.

Shipman, T., R. MacDonald, and T. Byrnes, 2018, Experiences and learnings from induced seismicity regulation in Alberta: Interpretation, **6**, SE15–SE21.

Walsh, F. R., and M. D. Zoback, 2016, Probabilistic assessment of potential fault slip related to injectioninduced earthquakes: Application to north-central Oklahoma, USA: Geology, **44**, 991–994.

Walsh, F. R., M. D. Zoback, D. Pais, T. Tyrrell, and M. Weingarten, 2017, FSP 1.0: A Program for Probabilistic Assessment of Fault Slip Potential From Fluid Injection.

Zhang, H., D. W. Eaton, G. Rodriguez, and S. Q. Jia, 2019, Source-Mechanism Analysis and Stress Inversion for Hydraulic-Fracturing-induced Event Sequences near Fox Creek, Alberta: Bulletin of the Seismological Society of America, **109**, 636–651.